Integrative Zoology 2021; 16: 712–728 doi: 10.1111/1749-4877.12551

ORIGINAL ARTICLE

INTEGRATIVE ZOOLOGY

Temperature and mass scaling affect cutaneous and pulmonary respiratory performance in a diving frog

Ryan B. MCWHINNIE, Jason P. SCKRABULIS and Thomas R. RAFFEL

Department of Biological Sciences, Oakland University, Rochester, Michigan, USA

Abstract

Global climate change is altering patterns of temperature variation, with unpredictable consequences for species and ecosystems. The Metabolic Theory of Ecology (MTE) provides a powerful framework for predicting climate change impacts on ectotherm metabolic performance. MTE postulates that physiological and ecological processes are limited by organism metabolic rates, which scale predictably with body mass and temperature. The purpose of this study was to determine if different metabolic proxies generate different empirical estimates of key MTE model parameters for the aquatic frog *Xenopus laevis* when allowed to exhibit normal diving behavior. We used a novel methodological approach in combining a flow-through respirometry setup with the open-source Arduino platform to measure mass and temperature effects on 4 different proxies for whole-body metabolism (total O_2 consumption, cutaneous O_2 consumption, pulmonary O_2 consumption, and ventilation frequency), following thermal acclimation to one of 3 temperatures (8°C, 17°C, or 26°C). Different metabolic proxies generated different mass-scaling exponents (b) and activation energy (E_A) estimates, highlighting the importance of metabolic proxy selection when parameterizing MTE-derived models. Animals acclimated to 17°C had higher O_2 consumption across all temperatures, but thermal acclimation did not influence estimates of key MTE parameters E_A and b. Cutaneous respiration generated lower MTE parameters than pulmonary respiration, consistent with temperature and mass constraints on dissolved oxygen availability, SA:V ratios, and diffusion distances across skin. Our results show that the choice of metabolic proxy can have a big impact on empirical estimates for key MTE model parameters.

Key words: African clawed frog, amphibian, pneumotachography, thermal biology

INTRODUCTION

Climate change is projected to increase mean temperatures and temperature variability, with potentially complex effects on species and the ecosystems they inhabit (Donelson *et al*. 2018; Morash *et al*. 2018; Burggren 2018). These changes are especially important for ectothermic animals including amphibians, which allow their core body temperatures to vary with environmental temperature. Understanding thermal responses is increasingly important for amphibians due to the global spread of temperature-dependent diseases (Berger *et al*. 1998; Stuart *et al*. 2004; Skerrat *et al*. 2007). Measuring how changes in temperature affect an organisms' physiological performance is crucial to identifying at-risk species and mitigating effects of anthropogenic climate change.

One of the most important tools for describing ectotherm thermal responses is the thermal performance

Correspondence: Ryan B. McWhinnie, Oakland University, Department of Biological Sciences, 375 Dodge Hall, 118 Library Drive, Rochester, MI 48309, USA.
Email: rbmcwhin@gmail.com

curve (TPC), which describes some metric of an organism's performance across a range of temperatures (Denny & Dowd 2012). TPCs are typically asymmetric and increase exponentially with temperature up to an organism's peak performance temperature (T_{pk}), above which performance rapidly declines (Denny & Dowd 2012). Due to this inherent non-linearity of TPCs, it is important to quantify performance across a range of temperatures and to describe the TPC using an appropriate mathematical model. Although a wide variety of models have been used to describe thermal performance curves, arguably the most mechanistic and potentially generalizable are equations derived from the metabolic theory of ecology (MTE). Brown (2004) presents central equations, assumptions, and the theoretical framework in a greater depth.

One advantage of MTE-derived models is the potential generalizability of key model parameters such as the activation energy E_A, which is predicted to have similar values across taxa and physiological processes (Brown *et al*. 2004; Dell *et al*. 2011). Most MTE-derived models are parameterized using some proxy for metabolic performance (e.g. sprint speed, ventilation frequency, or activity level), which is assumed to be proportional to the mass-specific metabolic rate *B* (Gillooly *et al*. 2001; Brown *et al*. 2004; Savage *et al*. 2007). However, this common assumption of a constant E_A across metabolic proxies remains to be tested for most ectotherm species. A second advantage of MTE-derived models is the ability to simultaneously describe temperature and mass-scaling effects on metabolism. Our goal in this study was not to test fundamental assumptions of MTE. Instead, we used MTE-derived models to simultaneously describe temperature and mass effects on respiratory performance in the model amphibian species *Xenopus laevis* (Daudin, 1802), and we tested the common empirical assumption of invariant E_A across multiple metabolic proxies. The first objective of this study was to estimate the E_A for whole-body metabolism of *X. laevis* and determine if different metabolic proxies generate similar E_A estimates.

An important aspect of TPCs is their ability to shift following extended exposure to a given temperature, due to developmental or reversible plasticity (i.e. thermal acclimation responses). Classic MTE studies tended to ignore acclimation effects on thermal performance curves (e.g. Gillooly *et al*. 2001), but more recent studies have suggested thermal acclimation can be incorporated into MTE by making key parameters into functions of recently experienced temperatures (Rohr *et al*. 2013). Depending on the type of response, acclimation temperature can have positive, negative, or non-linear effects on the thermal performance curve (Altman *et al*. 2016; Padilla *et al*. 2019). The "beneficial acclimation" hypothesis predicts that acclimation of an organism to a given temperature will result in increased performance at that temperature, relative to unacclimated organisms (i.e. adaptive plasticity; Leroi *et al*. 1994). This type of pattern is typical for acclimation effects on ectotherm thermal limits (e.g. increased critical thermal maximum following warm-temperature acclimation; Bilyk & DeVries 2011). Results consistent with beneficial acclimation were observed for locomotor performance in *X. laevis*, where cold-acclimated frogs had higher maximum sprint speeds at cold temperatures relative to their warm-acclimated counterparts (Wilson *et al*. 2000; Seebacher *et al*. 2014). However, not all organisms or performance metrics exhibit beneficial acclimation responses when measured at temperatures below their T_{pk}, instead exhibiting "cooler is better," "warmer is better," or "optimal temperature" responses (Wilson & Franklin 2002). The second objective of this study was to test for thermal acclimation effects on *X. laevis* metabolic performance and to determine if acclimation influence MTE parameter estimates. Based on the prior study on *X. laevis* swimming speed, we hypothesized a "beneficial acclimation" effect on *X. laevis* respiratory performance, which should be strongest immediately after a temperature shift and dissipate through time as each animal becomes acclimated to its new "performance" temperature.

Previous authors have demonstrated that within-species metabolic mass scaling relationships exhibit a wide range of exponents (here defined as parameter "*b*" in models), possibly due to differential reliance on specific physiological systems (reviewed by Glazier 2005, 2014a,b). For example, *X. laevis* is a diving frog that relies heavily on cutaneous respiration (gas exchange through the skin; Hutchison *et al*. 1968), which is temperature dependent and may be limited by the organism's surface area to volume ratio (SA:V; predicted scaling exponent of 2/3) or increased skin thickness in larger frogs (Rubner 1883; Greven *et al*. 1995; VanBuren *et al*. 2018). A prior study observed a mass-scaling exponent of 1.08 for *X. laevis* whole-body respiration, but frogs were taken out of their normal aquatic environment for measurements of oxygen consumption, possibly forcing them to rely more heavily than normal on pulmonary respiration (Hillman & Withers 1979). Furthermore, within-species mass scaling exponents have been found to change in response to temperature and thermal acclimation (Killen *et al*. 2010; Ohlberger *et al*. 2012). A third objective of this study was to estimate mass scaling exponents for *X. laevis* pulmonary, cutaneous, and whole-body respiration while

allowing animals to exhibit their normal diving behavior, and to determine if temperature or thermal acclimation influences mass scaling relationships in this species. We hypothesized a scaling exponent for total O_2 consumption close to 0.75 (Savage *et al*. 2008), and a higher exponent for pulmonary than for cutaneous respiration due to constraints imposed by SA:V and skin thickness in larger frogs.

The focal species of this study was the African clawed frog *Xenopus laevis*, an amphibian species commonly used as a model organism in biomedical research. *X. laevis* is a diving frog that poses a unique set of challenges when studying respiration, due to its heavy reliance on cutaneous respiration and ability to go extended periods without surfacing to breathe air (pulmonary respiration; Boutilier 1984). A common methodological approach has been closed system respirometry (Hutchison & Miller 1979; Feder 1983; Hastings & Burggren 1995). However, other authors used pneumotachography, a specialized type of air flow-through system, to track ventilation frequency and measure breath volumes for diving animals including *X. laevis* (Boutilier 1984; Hedrick *et al*. 2011; Withers *et al*. 2014). Previous studies also measured whole-body metabolic rates by placing each frog in a humid air chamber (i.e. terrestrial environment) to generate a single value for whole-body oxygen consumption (Seymour 1973; Hillman & Withers 1979) or carbon dioxide production (Tsugawa 1982), or took separate measurements of changing oxygen concentrations in air and water to estimate relative contributions of pulmonary versus cutaneous respiration (Emilio & Shelton 1974, 1980; Hillman & Withers 1981; Feder & Wassersug 1984). Costs and limitations of these various respirometry systems for experiments with diving frogs are discussed in more detail in Supporting Information. A fourth objective of this study was to develop an inexpensive flow-through system for simultaneous measurement of total O_2 consumption, pulmonary O_2 consumption, cutaneous O_2 consumption, ventilation frequency, and breath volumes while allowing frogs to exhibit their normal diving behavior.

This study aimed to answer 3 key questions: (1) How does *X. laevis* whole-body metabolism scale with body mass, and does this mass-scaling exponent depend on the choice of metabolic proxy, temperature, or thermal acclimation status? (2) What is the activation energy estimate for *X. laevis* whole-body metabolism, and does this estimate depend on choice of metabolic proxy or thermal acclimation? (3) How does thermal acclimation affect the metabolic thermal performance curve of *X. laevis*, and do these effects differ for different metabolic proxies? Answering these key questions will provide insights into the temperature dependence of *X. laevis* whole-body metabolism in a natural environment and help inform future studies of metabolic performance.

MATERIALS AND METHODS

Animal source and maintenance

All experiments were conducted in accordance with the Oakland University Institutional Animal Care and Use Committee (IACUC #18011).

Wild-type *Xenopus laevis* tadpoles (Nieuwkoop-Faber stages 56–63) were obtained in September of 2017 from a commercial research supplier (Nasco, Fort Atkinson, WI, USA) and raised to subadults (about 10 months old). The research supplier was unable to discern the strain of the species. All water quality parameters were maintained in accordance with optimal husbandry conditions presented by Green (2010). Groups of 15–30 tadpoles were housed in an opaque 2.4-gallon tank with gray-tinted translucent lids, to minimize potential distress from disturbance. Enrichment in the form of PVC pipes were used as refuge for social housing. Tanks were filled with 20°C Kordon Amquel®-treated water to slow the rate of water fouling. Animals were maintained on a 12:12 h light:dark cycle. Tadpoles were fed a crushed mix of "frog brittle" from the *Xenopus* supplier and changed daily. Subadults were housed in groups of 3 to 4 and fed3 times weekly with post-metamorphic brittle from the *Xenopus* supplier. All animals were checked daily for overall health and water quality.

Rationale for developing a custom flow-through system for diving-frog respirometry

We designed a new respirometry system to allow simultaneous measurement of cutaneous and pulmonary respiration in a diving frog, while allowing frogs to exhibit normal diving behavior. We based our design on a combination of respirometry strategies used by prior studies (Hillman & Withers 1979; Boutilier 1984; Fonseca *et al*. 2012; Tattersall *et al*. 2013). We considered it important to allow animals to exhibit normal diving behavior during respirometry measurements, to ensure that the relative contributions of cutaneous and pulmonary respiration (and their subsequent effects on overall MTE parameters) would be reflective of *X. laevis* in a more natural environment. We therefore chose not to force animals to

remain either fully submerged with no access to air or in a humid terrestrial chamber with no ability to submerge. Some prior studies used closed-system respirometry, in which O_2 concentrations are measured through time with no external source of oxygen, to track rates of cutaneous and pulmonary respiration in *X. laevis* (e.g. Hutchison & Miller 1979; Hillman & Withers 1979, 1981; Tattersall *et al*. 2013). However, we worried that depletion of atmospheric oxygen through time might influence *X. laevis* breathing behavior in our experiments, and we were concerned about possible toxicity of the mineral oil used by some prior studies to minimize oxygen diffusion between the air and water (e.g. Hillman & Withers 1981). We were also interested in tracking ventilation frequency and breath volumes as possible alternative metabolic proxies, which would not have been possible with closed system respirometry. We therefore sought a way to conduct flow-through respirometry for at least the pulmonary component of our respirometry system.

Some prior studies used pneumotachography to track breath rates and volumes in diving animals including *X. laevis* (Glass *et al*. 1983; Boutilier 1984; Fonseca *et al*. 2012). In these studies, animals were held within an upside-down funnel that restricted pulmonary respiration to a small "diving bell" (Glass *et al*. 1983; Boutilier 1984; Fonseca *et al*. 2012). Air was then pumped through the diving bell at a constant flow rate, which was measured using a pneumotachograph sensitive enough to pick up changes in flow rate caused by the animal's lung inspiration or expiration (e.g. Boutilier 1984). This setup has several advantages, in that it: (1) allows animals to exhibit their normal diving behavior, (2) ensures continuous access to freshly oxygenated air, (3) allows flow-through measurements of pulmonary O_2 consumption (e.g. Fonseca *et al*. 2012), and (4) provides opportunities to restrict oxygen diffusion between water and air by limiting the surface area of water where animals breathe. However, these studies utilized analog flow spirometers that have become difficult to obtain and would likely not have been sensitive enough to measure breath volumes of some of the smaller frogs in the current study. Furthermore, commercially available flow-through respirometry systems that measure O_2 consumption were cost-prohibitive for our experimental design, which required measuring 12 animals simultaneously in replicate controlled-temperature chambers. We therefore sought to combine classic pneumotachography methods with a digital device capable of simultaneously measuring both the air flow rate and the oxygen concentration in the flow-through air over time.

Respirometry setup and quantifying metabolic proxies

We designed a respirometry system to simultaneously measure cutaneous and pulmonary respiration in a diving frog, inside a controlled-temperature incubator (Fig. 1; Fig. S1, Supporting Information), based on a combination of respirometry strategies used by prior studies (Hillman & Withers 1979; Boutilier 1984; Fonseca *et al*. 2012; Tattersall *et al*. 2013). Each animal was placed into a 1 L deli cup within a commercial reptile incubator (Exo Terra, www.exo-terra.com) set to the target performance temperature. We inserted an upside-down perforated funnel (top half of a plastic pop bottle) into each deli cup to restrict each animal's air access to a small (7 mL) pocket at the top of the funnel. Funnels were size matched to the body length of each frog to ensure they could reach the surface without needing to swim, thereby reducing background "noise" generated by frog swimming movements. However, it is important to recognize that water depth can influence *X. laevis* surfacing frequency (Shannon & Kramer 1988), with unknown effects on mass or temperature scaling of respiratory variables. Thus, it is possible that deeper water, which requires frogs to swim or float to reach the surface, might generate different results from the current study.

We pumped a constant flow of air through this air pocket during each respirometry measurement, at a rate of approximately 200 $mL \bullet min^{-1}$, ensuring the air in the pocket was fully refreshed every 2–3 s. We connected the outgoing tube to our custom-built respirometry device to quantify of changes in air flow and oxygen percentages through time (Fig. 1). The device was sensitive enough to detect changes in air flow caused by frog inhalation and exhalation, each of which respectively decreased or increased the flow rate across the sensor, allowing us to count breaths through time and calculate individual breath volumes (Fig. S2, Supporting Information). Diving frogs like *X. laevis* typically have extended "gap" periods with no breaths punctuated by distinct periods of breathing activity (Boutilier 1984). Using Boutilier's (1984) terminology, we refer to these discrete periods of breathing activity as "breath bouts" and define one "breath" is a single cycle of inhalation and exhalation. We used these data to quantify pulmonary oxygen consumption for individual breaths and over the full measurement period. We also quantified cutaneous oxygen consumption by measuring changes in aqueous dissolved oxygen from the beginning to end of each measurement period. Additional details describing the respirometry setup and

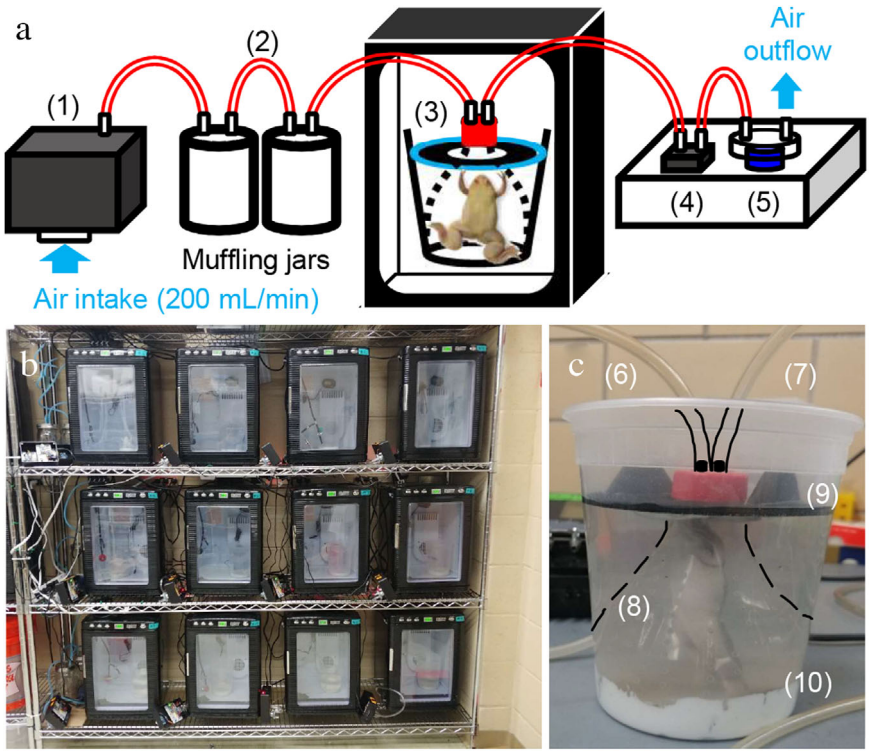

Figure 1 Complete respirometry setup. (a) Diagram of full respirometry setup including: (1) air intake pump, (2) a pair of quart-sized muffling jars used to minimize variation in flow rate going to the frog, (3) the frog within its pneumotachography setup (shown in panel "c"), (4) air flow-rate sensor, and (5) oxygen sensor covered by a modified plastic coin holder that channels air over the sensor. (b) Array of 12 incubators for performance temperature measurements of individual frogs. A black project box containing flow and O_2 sensors is visible to the left of each incubator, and muffling jars are visible to the left of each shelf. (c) Close-up photo of the pneumotachography setup for an individual frog including: (6) intake tubing for air going to frog, (7) outflow tubing from frog, (8) frog positioned vertically inside funnel (highlighted with dashed lines), (9) floating foam barrier to minimize oxygen diffusion between the water and air, and (10) sculpting clay to stabilize the funnel.

calculations for quantifying metabolic proxies can be found in Supporting Information.

Primary controlled-temperature experiment

Our primary experiment was designed to investigate effects of temperature and thermal acclimation on various metabolic proxies for *X. laevis*. A total of 24 subadult *X. laevis* were used for this study, though one frog died during the first acclimation period (i.e. maximum 23 frogs per experiment). We ran this experiment twice using the same set of frogs, re-randomizing each frog to a new temperature treatment combination prior to the second experiment. The mass and total body length (snout to tip of extended feet) of each frog was taken at the beginning and end of each 17-day acclimation period. Sizes varied from 13.13–59.95 g ($\underline{x} = 31.69$) for body mass and from 10.3–15.1 cm ($\underline{x} = 13.10$) for total body length at the start of performance measurements. We did not determine animal sex because frogs were too young to exhibit external characteristics of sexual maturity. Each of the 2 experiments was further divided into 2 temporal blocks for measurement purposes, since only a maximum of 12 frogs could be measured simultaneously. Experiment 1 (blocks 1 & 2) was conducted in late June of 2018 and experiment 2 (blocks 3 & 4) was conducted in late July of 2018. All measurements were conducted during typical workday hours, ranging from morning to midafternoon. Animals were randomly assigned to blocks and temperature treatments. Animal identifications were maintained throughout the entirety of this study, allowing us to control for random effects of individual frogs. Each experiment began with a 17-day acclimation period in which animals were acclimated to 8°C, 17°C, or 26°C. Within each temporal block, we measured frog respiration at 5 time points relative to the

end of the acclimation period: −1, 0, 1, 4, and 8 days. At the end of the acclimation period (day 0), each animal was shifted to one of 8 randomly assigned performance temperatures for respirometry measurements (8°C, 11°C, 14°C, 17°C, 20°C, 23°C, 26°C, and 29°C). During the performance period (0–8 day time points), performance temperatures were re-randomized for each respirometry measurement, with constraints to not repeat the same performance temperature for a given frog within each experiment. This experimental design minimized the possibility of frogs becoming acclimated to their new performance temperatures. Further experimental design details are provided in Supporting Information.

Post-experiment measurements

The primary controlled-temperature experiment included a sufficiently broad range of animal masses to reveal interesting differences in mass scaling coefficients among metabolic proxies (13.13–59.95; $\underline{x} = 30.65$). However, this mass range is less than the order of magnitude, which might result in inaccurate intraspecific estimates of parameter "*b*" due to the potential for curvilinear mass-scaling relationships (Savage *et al*. 2008). To generate more accurate estimates of *b* for various metabolic proxies, we collected additional measurements from 8 recently metamorphosed *X. laevis* frogs in a smaller size range (1.87–3.18 g, $\underline{x}= 2.66$). To obtain comparable measurements, we randomly assigned each frog to one of the performance temperatures from the original controlled-temperature experiment.

Statistical analyses

All statistical analyses were based on linear mixed-effects regression (*lmer* function from the *lme4* package) and conducted using R statistical software v. 3.5.1 (R Core Team 2018), allowing us to incorporate random effects of Acclimation incubator, Performance incubator, and Frog identity into statistical models. The random effect of Frog identity was nested within the effect of Acclimation incubator. We natural log-transformed all response variables (i.e. our 4 metabolic proxies) and used the inverse of performance-temperatures (in degrees Kelvin) as a primary explanatory variable, to allow estimation of E_A from linear-model outputs both in the overall controlled-temperature experiment and for each individual time point. We also included natural log-transformed body mass as a covariate in each model, to account for mass-scaling effects and to allow estimation of the mass-scaling exponent (*b*) for each metabolic proxy. For analysis of the primary controlled-temperature experiment, we also tested for curvilinear and interactive effects of acclimation temperature and time since the temperature shift. Further details about model structure are provided in Supporting Information Supplementary Methods.

To determine if MTE parameter estimates depended on the size range of animals included in the analysis, we re-ran linear mixed effects models with and without inclusion of post-experiment measurements collected from frogs in a smaller size range. These models were simplified to remove fixed effects of acclimation temperature or time because all of the smaller frogs used for post-experiment measurements had been acclimated to the same temperature (19°C). However, we retained the random-effects structure from the original mixed-effects models. The new frogs were all assigned to the same "acclimation incubator" for the purpose of accounting for this random effect, since they were maintained on the same shelf in our animal room prior to conducting measurements.

RESULTS

Acclimation effects on thermal performance

To test for potential linear or curvilinear effects of acclimation temperature on each metabolic proxy, we focused on data from time points following the acclimation period. We began by testing for time by temperature interactions using the full time series (days 0–8; Table 1; Fig. S3, Supporting Information). We detected a statistically significant positive 3-way interaction for effects of inverse performance temperature × time × quadratic acclimation temperature on total O_2 consumption. We also detected a significant quadratic acclimation temperature × time interaction for total O_2 consumption, revealing negative curvilinear effects of acclimation at a large time scale. Cutaneous respiration also generated a significant positive quadratic acclimation × time interaction (Table 1). A main effect of time on ventilation frequency was statistically significant, revealing that ventilation frequency increased through time post-acclimation (Table 1). We next conducted a series of focused models examining each individual time point (days 0, 1, 4, and 8), to determine if acclimation effects were stronger at time points immediately following the temperature shift (Table S1 and Fig. S4, Supporting Information). Immediately following the temperature shift, there was a trend towards a quadratic effect of acclimation on total oxygen consumption ($P = 0.088$; Table S1, Supporting Information; Fig. 2a). These patterns were supported by highly significant interactions

Table 1 Linear mixed-effects models testing for effects of acclimation through time (days 0–8), in the primary controlled-temperature experiment

Response	Predictor	Coef ± SE	*F*	df	*P*
Total O_2	$PerfTemp^{-1}$	0.458 ± 0.029	260.2	1, 157.0	<0.001
	AccTemp	0.003 ± 0.006	0.1	1, 7.6	0.783
	$AccTemp^2$	$-3.55 \times 10^{-4} \pm 0.001$	0.1	1, 7.0	0.751
	ln Mass	0.430 ± 0.124	10.6	1, 37.6	0.002
	Time	0.006 ± 0.007	0.8	1, 137.0	0.381
	$PerfTemp^{-1} \times AccTemp$	19.1 ± 44.2	0.3	1, 161.8	0.610
	$PerfTemp^{-1} \times AccTemp^2$	6.25 ± 8.61	0.6	1, 158.7	0.458
	$PerfTemp^{-1} \times Time$	0.732 ± 115.0	0.0	1, 151.5	0.953
	$AccTemp \times Time$	$8.36 \times 10^{-4} \pm 0.001$	0.7	1, 145.1	0.405
	$AccTemp^2 \times Time$	$6.67 \times 10^{-4} \pm 2.01 \times 10^{-4}$	10.8	1, 147.5	0.001
	$PerfTemp^{-1} \times AccTemp \times Time$	−0.101 ± 15.32	0.0	1, 171.2	0.976
	$PerfTemp^{-1} \times AccTemp^2 \times Time$	7.37 ± 3.50	3.9	1, 107.8	0.049
Cutaneous O_2	$PerfTemp^{-1}$	0.278 ± 0.020	196.1	1, 181.0	<0.001
	AccTemp	0.006 ± 0.004	2.0	1, 8.6	0.193
	$AccTemp^2$	$-4.48 \times 10^{-4} \pm 8.16 \times 10^{-4}$	0.3	1, 7.5	0.610
	ln Mass	0.270 ± 0.085	8.9	1, 37.2	0.005
	Time	0.012 ± 0.005	4.9	1, 155.7	0.029
	$AccTemp \times Time$	$1.04 \times 10^{-4} \pm 7.20 \times 10^{-4}$	0.1	1, 98.6	0.739
	$AccTemp^2 \times Time$	$4.27 \times 10^{-4} \pm 1.40 \times 10^{-4}$	9.0	1, 160.8	0.003
Pulmonary O_2	$PerfTemp^{-1}$	0.794 ± 0.066	119.2	1, 168.6	<0.001
	AccTemp	−0.004 ± 0.012	0.1	1, 9.5	0.760
	ln Mass	0.768 ± 0.238	9.3	1, 39.3	0.004
	Time	0.004 ± 0.017	0.1	1, 138.2	0.803
Ventilation frequency	$PerfTemp^{-1}$	0.365 ± 0.062	26.0	1, 215.8	<0.001
	AccTemp	−0.018 ± 0.012	2.0	1, 9.7	0.188
	ln Mass	0.098 ± 0.247	0.1	1, 39.8	0.709
	Time	0.042 ± 0.016	6.9	1, 140.4	0.010

Statistical tests are based on linear mixed effects regression, using *F*-tests with type II sums of squares and Kenward-Rogers df. All models included random effects of performance incubator, acclimation incubator, and frog identity. Final models were selected using backwards selection, with non-significant interaction terms removed ($P > 0.05$). Time was measured from the day each frog was moved to its final performance temperature (0, 1, 4, and 8 days). Predictor coefficients were taken from models with only marginal terms removed, to ensure they could be used to interpret main effect directionalities. $PerfTemp^{-1}{}_A$ estimates in other tables. Coefficients were multiplied by −k for comparison with E_A.

between time and the quadratic effect of acclimation temperature for total oxygen consumption and cutaneous respiration, consistent with an "optimum temperature"-type acclimation pattern.

No other metabolic proxies revealed significant acclimation effects on day 0. A statistically significant positive effect of acclimation was detected on day 1 for cutaneous respiration (Table S1, Supporting Information). Cold-acclimated animals had the lowest levels of cutaneous respiration across performance temperatures, which likely drive this pattern (Fig. 2b).

We detected a strong negative trend of acclimation effects on ventilation frequency at 1 day into the performance period (Table S1, Supporting Information), with warm-acclimated animals having lower ventilation frequency levels across all performance temperatures. No

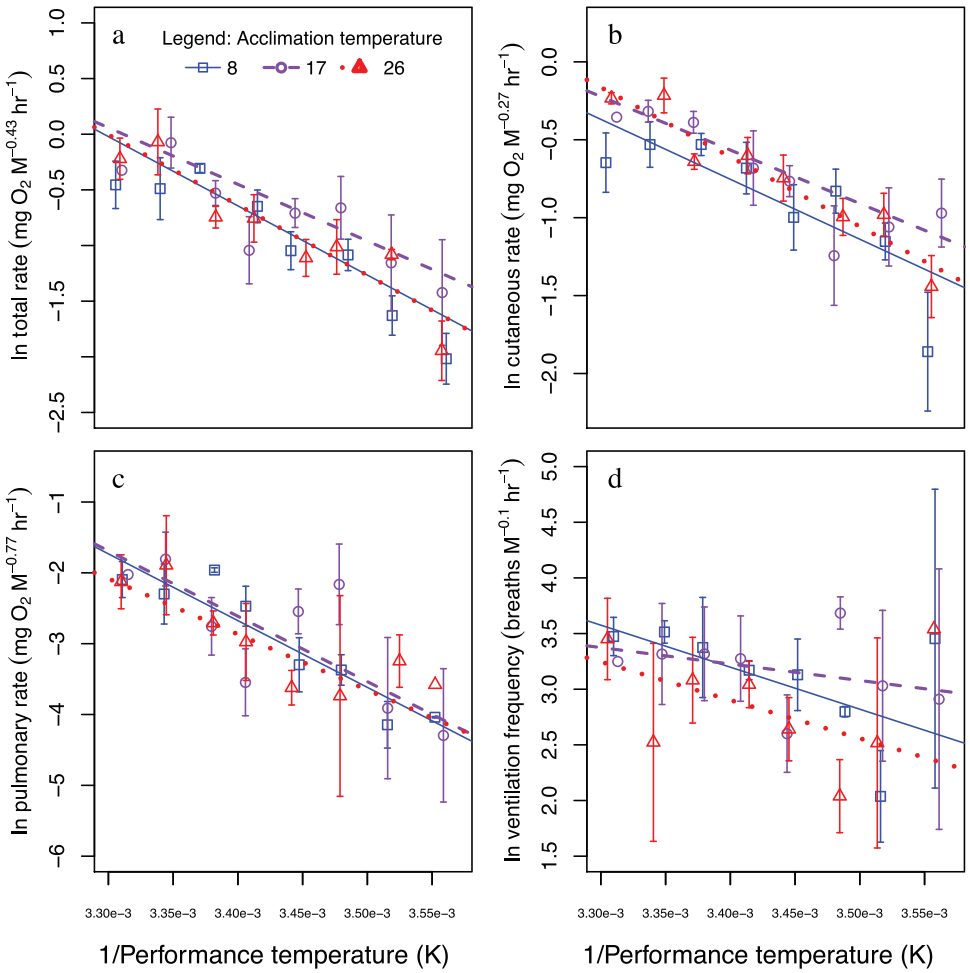

Figure 2 Thermal performance curves for all metabolic proxies on day zero of the primary controlled-temperature experiment (i.e. immediately following the shift from acclimation temperatures). (a) Total respiration ($N = 75$). (b) Cutaneous respiration ($N = 81$). (c) Pulmonary respiration ($N = 72$). (d) Ventilation frequency ($N = 72$). All response variables were natural log transformed and scaled according to the observed mass scaling effects. Note that the lines for cold- and warm-acclimated animals overlap in panel (a). Error bars represent the standard error of each treatment group containing $N > 1$ replicates.

significant effects of acclimation were detected for any metabolic proxy at 4 or 8 days following the temperature shift (Table S1, Supporting Information).

MTE parameter estimates: mass scaling exponents (b) and activation energies (E_A)

To maximize the number of measurements used to generate estimates of key MTE parameter estimates (overall b and E_A values), we used data collected at all time points post-acclimation, including measurements from the primary controlled-temperature experiment and additional measurements of 8 smaller frogs. Parameter estimates are provided as mean followed by 95% confidence intervals. All 4 metabolic proxies increased with body mass, resulting in positive mass scaling exponents (Fig. 3; Table S2, Supporting Information). Pulmonary respiration had a higher mass-scaling exponent ($b = 1.565$; 95% CI 1.311–1.819) than cutaneous respiration ($b = 0.472$; 0.372–0.571), resulting in an intermediate value for total O_2 consumption ($b = 0.690$; 0.576–0.803). Ventilation frequency generated the lowest mass-scaling exponent ($b = 0.225$; 0.004–0.445). We detected no statistically significant interactions of mass with either acclimation or performance temperature. Final estimates of mass-scaling exponents for pulmonary, cutaneous, and total respiration all increased with addition of the 8 smaller frogs,

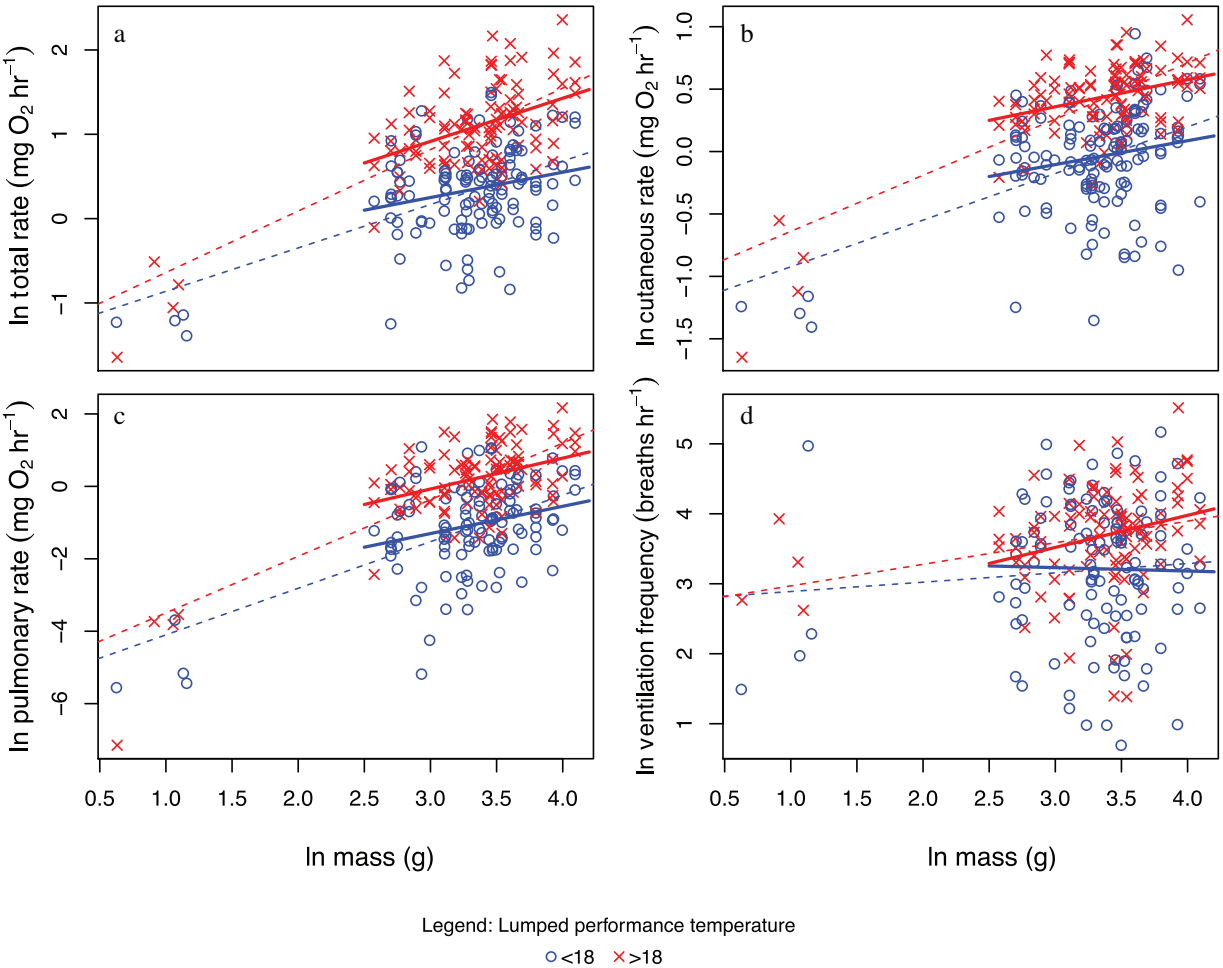

Figure 3 Plots of all 4 metabolic proxies as a function of frog mass on a log-log scale for all measurements, including 8 smaller frogs that were not part of the original controlled-temperature experiment. (a) Total O_2 consumption ($N = 236$), (b) cutaneous O_2 consumption ($N = 257$), (c) pulmonary O_2 consumption ($N = 236$), and (d) ventilation frequency ($N = 237$). Data are grouped according to performance temperature (<18°C: blue circles; >18°C: red crosses). Note that best-fit lines were generated using simple linear regression to illustrate trends and do not account for random effects, unlike the statistical models we used to estimate MTE parameters. Solid lines were generated based on the original dataset from the primary controlled-temperature experiment. Dashed lines were generated using the full dataset.

relative to estimates based only on data from the primary controlled-temperature experiment (Table S2, Supporting Information).

Total O_2 consumption (pulmonary plus cutaneous) and ventilation frequency yielded intermediate E_A estimates of 0.444 eV (0.389–0.499) and 0.373 eV (0.250–0.496), respectively (Table S2, Supporting Information). Pulmonary respiration yielded the highest overall E_A estimate (0.770 eV; 0.640–900) relative to other metabolic proxies, whereas cutaneous respiration alone yielded the lowest estimate (0.270 eV; 0.213–0.309). Ventilation frequency revealed a trend towards a curvilinear performance temperature × quadratic effect of acclimation temperature interaction ($F_{1,155.8} = 3.0$; $P = 0.088$; Table 1), driven by an apparently lower E_A for 17°C-acclimated frogs (0.102 eV; −0.144–0.348) relative to cool-acclimated (8°C: 0.488 eV; 0.306–0.669) or warm-acclimated frogs (26°C: 0.444 eV; 0.231–0.657). Unlike with the mass-scaling exponents, additional measurements from frogs in a smaller size range had little effect on the estimated E_A for any of the 4 metabolic proxies (Table S2, Supporting Information).

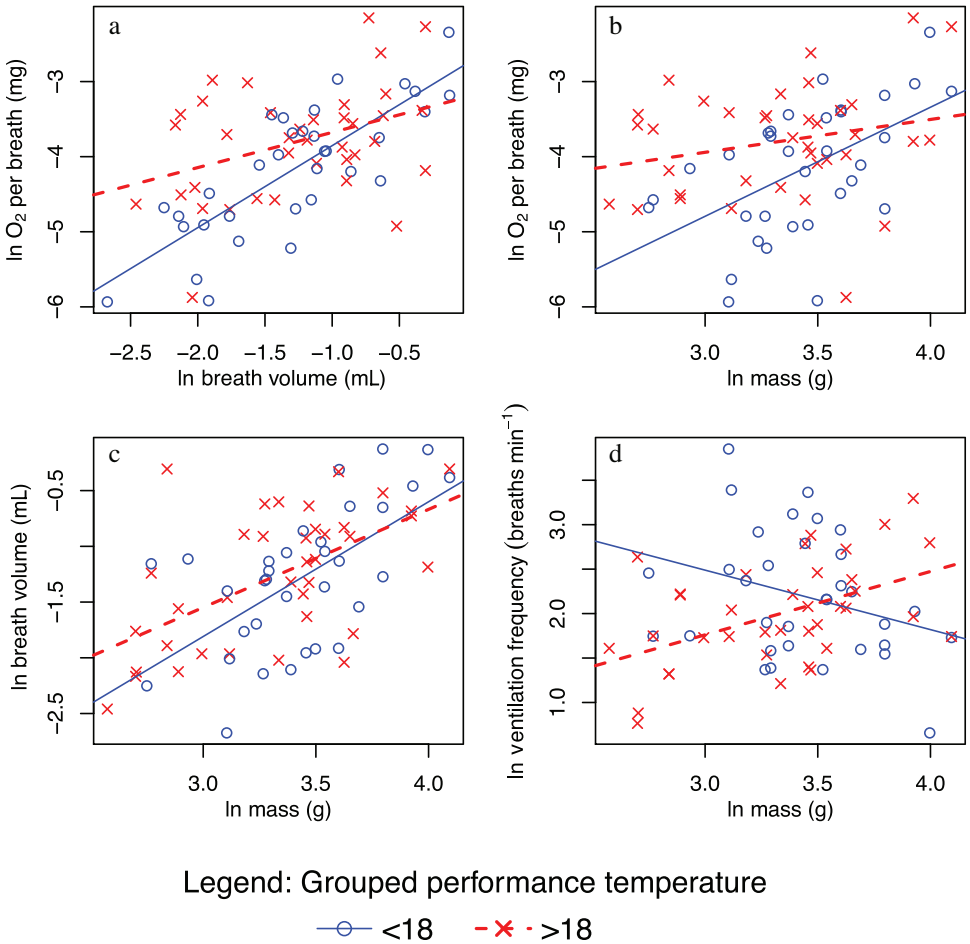

Figure 4 Mass- and volume-scaling relationships on a per-breath log-log scale, for breath bout data from the primary controlled-temperature experiment. Performance temperatures are grouped ("Cool" temperatures [8°C, 11°C, 14°C, and 17°C]; "Warm" temperatures [20°C, 23°C, 26°C, and 29°C]) for ease of data visualization. Panels show relationships between: (a) Breath volume and oxygen consumption ($N = 65.7$); (b) mass and oxygen consumption ($N = 38.7$). (c) Mass and breath volume ($N = 38.6$); (d) mass and ventilation frequency (breaths per minute; $N = 38.6$).

Mass- and volume-scaling relationships for individual breaths

To examine scaling relationships between breath volume, pulmonary O_2 consumption, and body mass in the original controlled-temperature experiment, we generated a separate dataset to focus on individual breath bouts for a given frog. We used this dataset to analyze scaling patterns for individual breath, providing an indirect way to assess how well breath volume might have worked as a fifth metabolic proxy. We first examined the scaling relationship between individual breath volume and O_2 uptake per breath to determine whether these variables were directly correlated with each other. However, this analysis revealed a strong interaction between breath volume and performance temperature, indicating that the scaling relationship between these 2 parameters was temperature-dependent (Table S3, Supporting Information). Oxygen uptake per breath increased faster with breath volume at cooler temperatures than at warmer temperatures (Fig. 4a; Table S4, Supporting Information). Given the absence of a temperature effect on the scaling exponent for overall pulmonary respiration through time (Table 1), this result initially seemed to suggest that using breath volume through time as a metabolic proxy might have generated a temperature-dependent mass scaling relationship.

We followed up on this result by examining relationships between log-transformed body mass (M), O_2 uptake

per breath, individual breath volume, and ventilation frequency within the breath bout dataset. Temperature interacted with ln(M) to affect O_2 uptake per breath (Fig. 4b; Table S3, Supporting Information), paralleling the interactive effects of temperature and breath volume on O_2 uptake per breath (Fig. 4a; Table S3, Supporting Information). In both cases, the interaction was driven by smaller frogs (or smaller breaths) absorbing more O_2 per breath at warmer than at cooler temperatures. In contrast, temperature did not significantly interact with the ln(M) effect on individual breath volume (Table S3, Supporting Information), although we detected a trend toward a ln(M) × performance temperature interaction ($P = 0.081$). Furthermore, ln breath volume was almost directly proportional to ln(M) with a scaling coefficient statistically indistinguishable from 1.0 (Table S3, Supporting Information). These results indicate that the temperature × breath volume interaction was driven by increased O_2 uptake at warmer temperatures for smaller frogs, rather than a temperature effect on individual breath volumes.

We also examined potential effects of acclimation and performance temperature on relationships between individual breath volume, oxygen uptake per breath, body mass (M), and ventilation frequency in the breath bout dataset (Table S3, Supporting Information; Fig. 4). The only statistically significant effect of acclimation temperature in the individual-breath analyses was a positive main effect on ventilation frequency ($P = 0.040$) after accounting for the effect of mass and performance temperature. Performance temperature decreased the scaling exponents for effects of both individual breath volume (Fig. 4a) and body mass (Fig. 4b) on oxygen uptake per breath, as indicated by significantly negative interactive effects between ln(M) or ln(V_{Breath}) and performance temperature (Table S3, Supporting Information).

There was no significant interactive effect of ln(M) and performance temperature on individual breath volume (Fig. 4c; Table S3, Supporting Information). In contrast, performance temperature increased the scaling exponent for the effect of body mass on ventilation frequency (Fig. 4d), as indicated by a significantly positive interactive effect of ln(M) and performance temperature on ventilation frequency in the breath bout dataset (Table S3, Supporting Information). Note that this same interactive effect of ln(M) and performance temperature was not significant in a separate mass-scaling analysis of individual breaths with the full dataset (discussed above; Table 1), though there was a trend towards a similar interactive effect in the same direction.

Observations of breathing behavior

Frogs exhibited patterns of breathing behavior similar to those observed in previously published experiments. Individual ventilations typically started with an exhalation followed by an immediate inhalation, as described by Brett and Shelton (1979; Fig. S2c, Supporting Information). As described by Boutilier (1984), frogs tended to ventilate their lungs multiple times each time they surfaced for air, with some frogs remaining near the surface and breathing in regular bouts ("bout breathing" behavior; Fig. S5a, Supporting Information) and others surfacing for a rapid succession of many ventilations following long periods without breathing ("burst breathing" behavior; Fig. S5b, Supporting Information). In general, frog breath rates tended to be faster at warmer temperatures and for larger frogs, across a range of breath rates consistent with those observed by Boutilier (1984; Table S5, Supporting Information).

DISCUSSION

Mass scaling exponents

Metabolic mass-scaling relationships varied depending on the metabolic proxy examined (Table 1) and the mass range of the frogs examined (Table S2, Supporting Information). The most direct measurement for whole-body metabolism in this study was total oxygen consumption, for which the full dataset generated a mass scaling exponent (b) similar to the MTE-predicted $M^{0.75}$ power law (Brown *et al*. 2004; $b = 0.690$; 95% CI 0.576–0.803). This estimate approximates the mean scaling coefficient observed in other empirical studies of intraspecific mass scaling (Hutcison *et al*. 1968). This scaling exponent for total respiration was intermediate between the estimates for cutaneous ($b = 0.472$; 0.372–0.571) and pulmonary ($b = 1.565$; 1.311–1.819) respiration. All 3 of these estimates were substantially increased when we added measurements from smaller frogs that were not part of the original controlled-temperature experiment (Table S1, Supporting Information), consistent with prior observations of convex curvature for intraspecific mass-scaling relationships and emphasizing the importance of including at least an order of magnitude range of masses when estimating intraspecific mass scaling parameters (Table S2, Supporting Information; Fig. 3; Savage *et al*. 2008).

We observed the largest mass-scaling exponent (b) for pulmonary oxygen consumption, which also exhibited the greatest increase in b with addition of the smaller frogs (Table S2, Supporting Information). This is apparently because larger frogs relied much more heavily on

pulmonary respiration than smaller frogs (Fig. S6, Supporting Information). This makes biological sense, because larger frogs have a lower surface-area to volume (SA:V) ratio than smaller frogs and should be less able to meet their oxygen demands via cutaneous respiration alone. As frogs get larger and rely more heavily on pulmonary respiration, you would expect the pulmonary scaling coefficient to begin converging on the overall *b* for total oxygen consumption. This is essentially what we saw when we focused on the larger frogs from the original experiment: a scaling coefficient for pulmonary respiration only slightly higher than 0.75 (Table S2, Supporting Information).

Cutaneous-only respiration generated a mass-scaling exponent that was lower than total or pulmonary respiration, and somewhat lower that the $M^{2/3}$ exponent predicted by a classic surface-area to volume (SA:V) scaling relationship (Rubner 1883; White & Seymour 2003; Table 1). A combination of biological factors likely influenced this depression in the mass-scaling exponent relative to other metabolic proxies. Gillooly *et al*. (2016) showed that mass scaling exponents for respiration are generally limited by how the respiratory surface area (i.e. skin surface area) and diffusion distance (i.e. skin thickness) scale with mass, with *b* equaling the difference between these 2 exponents. To our knowledge, there is no published work that simultaneously measured body mass, skin surface area, and skin thickness (or any combination of these 2 variables) in *X. laevis*, so we were unable to directly compare the mass scaling exponent for cutaneous respiration to exponents for surface area or skin thickness. However, *X. laevis* has a body shape similar to other anurans rather than possessing specific adaptations to increase skin surface area, and Hutchison *et al*. (1968) found that the average mass-scaling exponent for surface area across several anuran species was $M^{0.58}$. This is lower than the theoretical surface area to volume *b* of 0.67 for a spherical object (Rubner 1883), and only slightly outside the 95% c.i. for the cutaneous-respiration scaling coefficient observed in this study. Furthermore, *X. laevis* skin thickness appears to increase with body size, based on prior studies showing that females have both larger body mass and thicker skin than males (Greven *et al*. 1995; VanBuren *et al*. 2018). Based on these findings, a combination of SA:V and skin-thickness scaling relationships can likely account for the lower-than-expected mass-scaling exponent for cutaneous respiration observed in this study.

As expected, ventilation frequency generated the lowest *b* for all 4 metabolic proxies (Table 1; Table S2, Supporting Information). Because ventilation frequency is a mass-specific metabolic process, MTE predicts that the mass-scaling exponent should be 1.0 less than that for whole-body metabolic rate. In the present study, we predicted that the ventilation frequency mass-scaling exponent would be 1.0 less than the pulmonary mass-scaling exponent because these 2 metabolic proxies are inherently interrelated (i.e. $1.57 - 1.0 = 0.57$). The estimate of the *X. laevis* ventilation frequency exponent was somewhat smaller than this predicted value, though with overlapping confidence intervals (0.311–0.819 vs 0.004–0.445; Table S2, Supporting Information). One potential reason for discrepancies between the pulmonary and ventilation frequency mass-scaling exponents is that there was a substantial amount of noise in the flow rate time-series data, usually caused by sudden animal movements within the respirometry setup. These fluctuations generally lacked the distinguishing characteristics of real breaths, but they also frequently obscured real breaths, making it difficult to obtain accurate breath counts from the full time series of many frogs. As a result, this was an important source of measurement error in the "breath bout" dataset derived from the full time series for each frog. This noise also prevented us from obtaining accurate measurements of total ventilation volume through time, which we originally planned to analyze as a fifth metabolic proxy. We therefore explored the potential use of ventilation volume as an alternative metabolic proxy by examining mass-scaling relationships for the volume of individual breaths using the breath bout dataset, as described below.

All 4 metabolic proxies here analyzed generated different estimates of *b* for *X. laevis*, emphasizing the importance of selecting an appropriate metabolic proxy when investigating mass-scaling relationships for whole-body metabolism. However, these differences were qualitatively consistent with MTE predicted mass scaling relationships, and they might have been possible to predict quantitatively given sufficient information about how *X. laevis* skin surface area and thickness change with body mass (Gillooly *et al*. 2016). Importantly, there were no significant effects of temperature or thermal acclimation on mass-scaling exponents derived from any of the 4 metabolic proxies.

Mass- and volume-scaling relationships for individual breaths

If temperature influences the mass-scaling relationship for O_2 uptake per breath (Fig. 4a,b), then why did we not see a similar temperature-dependence for the mass scaling of pulmonary respiration in our full analysis (Fig. 3c)? The answer seems to have been that temperature had the

opposite interactive effect on the mass-scaling relationship for ventilation frequency, at least within the breath bout dataset (Table S4, Supporting Information; Fig. 4d). Indeed, reexamination of the ventilation frequency analysis from the full dataset revealed a similar trend towards temperature-dependent mass scaling (Fig. 3d), though this effect was non-significant (Table 1). These effects of temperature on b for O_2 per breath and ventilation frequency appear to have canceled each other out, with smaller frogs absorbing more O_2 per breath at warmer temperatures but breathing less frequently (Fig. 4b,d), ultimately resulting in a temperature-independent b for pulmonary O_2 consumption through time (Fig. 3c).

Activation energy estimates

As expected, activation energy estimates for all metabolic proxies fell within the reported range of 0.1–1.0 across taxa (Gillooly *et al*. 2001; Brown *et al*. 2004), with no statistical evidence for thermal acclimation effects on E_A. This finding corroborates current prominent MTE literature (Dell *et al*. 2011). Importantly, E_A estimates remained similar whether or not our analysis included the smaller frogs whose measurements were obtained after the primary controlled-temperature experiment (Table S2, Supporting Information). However, we found that estimates of the key metabolic parameter E_A varied considerably for *X. laevis* depending on which metabolic proxy we focused on. Most prior studies have generated E_A estimates based on only one metabolic proxy at a time (Nagano & Ode 2014). Obtaining different activation energies for the same species based different performance metrics might be interpreted to reflect fundamental differences in the temperature-dependence of different physiological processes, perhaps due to the involvement of different rate-limiting enzymes. However, results from the current study suggest that even direct measures of oxygen consumption can generate divergent estimates for the same organism's metabolic activation energy, particularly if one fails to account for all sources of oxygen (e.g. cutaneous versus pulmonary respiration). Based on this and prior studies for *X. laevis* and other amphibians (Whitford 1973; Hutchison & Miller 1979), reliance on pulmonary respiration increases at warmer temperatures, likely due in part to decreased dissolved oxygen availability in water at warmer temperatures (Fig. S7, Supporting Information; Keeling & Garcia 2002). This resulted in pulmonary oxygen uptake increasing with temperature more rapidly than cutaneous oxygen uptake, leading to a subsequently higher E_A estimate for pulmonary respiration.

Ventilation frequency also generated an intermediate E_A estimate, similar to total O_2 consumption. This was contrary to our a priori prediction that ventilation frequency would generate an E_A estimate similar to that of pulmonary oxygen uptake because of close biological relationship between these 2 metabolic proxies. This discrepancy is at least partly explained by our finding that frogs absorbed more oxygen per breath at warmer temperatures than at cooler temperatures, as revealed by positive main effect of temperature in the breath bout analysis. This effect might somewhat decrease the need for faster ventilation frequencies at warmer temperatures, relative to the need for increased pulmonary oxygen resulting in a lower E_A estimate for this proxy.

Acclimation effects on thermal performance

We found evidence of an optimal temperature-type thermal acclimation effect on the *X. laevis* whole-body metabolic rate, based on an analysis of total O_2 consumption (Table 1). This acclimation effect could be modeled in an MTE framework by allowing the normalization constant to be a function of acclimation temperature, as suggested by Gillooly *et al*. (2006). Overall, frogs acclimated to 17°C had higher O_2 consumption on day 0 than those acclimated to 8°C or 26°C (Fig. 2a), and this effect decreased through time following the temperature shift as indicated by a significant interaction between time and the quadratic effect of acclimation temperature (Fig. S4, Supporting Information; Table 1). However, the magnitude of this acclimation effect was weak and not statistically significant for individual time points, despite a strong trend towards a quadratic effect of acclimation temperature on day 0 (Table S1, Supporting Information). Analysis of other metabolic proxies revealed similar evidence of acclimation responses for cutaneous but not pulmonary O_2 consumption, suggesting that any effects of thermal acclimation on total O_2 consumption were driven by changes in cutaneous respiration.

This evidence for an optimal temperature-type acclimation response contrasts with results of prior studies, which measured acclimation effects on swimming speed and muscle power in *X. laevis* (Wilson *et al*. 2000; Seebacher *et al*. 2014). Both studies found evidence of higher performance by cold-acclimated animals when measured at cooler temperatures, consistent with either a beneficial acclimation or a cooler-is-better type response. Neither study included a third acclimation temperature, leaving open the possibility that either study might have detected decreased performance at even colder temperatures (i.e. an optimal temperature response). However,

"cold acclimation" occurred at 10°C in Wilson *et al*. (2000) and 15°C in Seebacher *et al*. (2014), and in both cases, cold-acclimated frogs outperformed warm-acclimated (25°C) frogs at cooler performance temperatures. In contrast, frogs acclimated to 8°C and 25°C in the current study appear to have had similarly low metabolic performance compared to 17°C acclimated frogs. These different results suggest that thermal acclimation has different effects on specific physiological processes (e.g. muscle performance) than on whole-body metabolic performance.

CONCLUSIONS

The results of this study show that the choice of metabolic proxy can influence estimates of key MTE parameters, and that *X. laevis* metabolic performance is influenced by thermal acclimation. All observed E_A estimates fell within the reported range for most animal taxa (Gillooly *et al*. 2001; Brown *et al*. 2004) but varied depending on the metabolic proxy examined, with pulmonary respiration generating a higher E_A value than cutaneous respiration due to a shift from cutaneous to pulmonary respiration at warmer temperatures. We also found evidence of an optimal-temperature type acclimation effect on the *X. laevis* whole-body metabolic rate, with higher total and cutaneous O_2 consumption in frogs acclimated to an intermediate temperature. This study also emphasizes the importance of allowing animals to exhibit normal respiratory behavior when studying mass and temperature effects on metabolic rates.

The observed mass-scaling exponent for total O_2 consumption of *X. laevis* was statistically indistinguishable from the MTE-predicted value of 0.75 (Gillooly *et al*. 2006), and the observed mass-scaling exponent for cutaneous respiration was only slightly less than the mean SA:V scaling exponent observed in a prior studies of frog morphology (0.58; Hutchison *et al*. 1968). This finding suggests that *X. laevis* cutaneous respiration is limited by skin surface area and SA:V ratios, and that larger frogs compensate for reduced SA:V by relying more on pulmonary respiration. Most prior studies of allometric scaling in diving animals focused on amniote vertebrates, which rely exclusively on pulmonary respiration (Schreer & Kovacs 1997; Halsey *et al*. 2006), though a prior study of bullfrogs also showed that increased temperatures led to greater reliance on pulmonary O_2 uptake and CO_2 elimination (Gottlieb & Jackson 1976). It would be interesting to examine *b* in other air-breathing diving species with significant cutaneous respiration (e.g. other aquatic frogs and salamanders) to determine if this is a common adaptation to a diving lifestyle. All of our estimated mass scaling exponents increased after incorporating additional measurements of smaller frogs. This result highlights the importance of including a wide range of masses for estimating intraspecific mass-scaling coefficients (Glazier 2005, 2010), preferably more than 1 order of magnitude as recommended by Savage *et al*. (2008). Had we stuck with the original mass range (13–60 g; about fivefold), we would have substantially underestimated the mass scaling estimates for all of our metabolic proxies. Including the additional measurements of smaller frogs makes these findings more robust and generalizable, for potential comparison with other diving species that exhibit significant amounts of cutaneous oxygen consumption.

The Arduino-based respirometry device developed in this study provides a powerful new experimental tool that may facilitate future experimental work. In the current study, this device made it possible to conduct flow-through respirometry with up to 12 animals simultaneously, facilitating quantification of metabolic thermal performance curves and acclimation effects. Furthermore, we were able to quantify breath volumes and oxygen uptake for individual breaths, allowing examination of allometric relationships at an individual breath level. Importantly, all measurements were collected while allowing animals to exhibit their normal diving behavior, generating more ecologically relevant estimates for *b* and E_A than would otherwise have been possible. Future researchers may find new ways to apply these tools to answer questions that might otherwise have been experimentally intractable.

ACKNOWLEDGMENTS

We thank the editor for their feedback and ultimately pushing us to produce a more robust and impactful contribution. The authors would also like to thank A. Orille, H. Russell, S. Pelton, B. Walter, K. Julius, J. Williams, and L. Trumbore for assisting with animal maintenance and preliminary experiments; A. Orille, S. Pelton, B. Walter, and M. Ostrowski for assisting with primary data collection; H. Russell, C. Evans, and B. Walter for assisting with data processing and compilation; and K. McWhinnie, S. Carell, J. Krasinski, R. Wilson, and J. Fischer for moral support. This work was supported by an NSF-CAREER grant to T.R.R. (IOS-1651888).

AUTHOR CONTRIBUTIONS

Conceptualization: T.R., R.M., and J.S. Methodology: T.R., R.M., and J.S. Analysis: R.M., T.R., and J.S.

Respirometry device construction: J.S. and R.M. Writing: R.M., J.S., and T.R. Funding acquisition: T.R.

COMPETING INTERESTS

The authors declare no competing or financial interests.

DATA AVAILABILITY STATEMENT

Data will be deposited to GitHub repository upon acceptance at www.github.com/jasonsckrabulis/mcwhinnie_etal_respirometry

REFERENCES

Altman KA, Paull SH, Johnson TJ *et al*. (2016). Host and parasite thermal acclimation responses depend on the stage of infection. *Journal of Animal Ecology* **85**, 1014–24.

Berger L, Speare R, Daszak P *et al*. (1998). Chytridiomycosis causes amphibian mortality associated with population declines in the rain forests of Australia and Central America. *PNAS* **95**, 9031–6.

Bilyk KT, DeVries AL (2011). Heat tolerance and its plasticity in Antarctic fishes. *Comparative Biochemistry and Physiology* **158**, 382–90.

Boutilier RG (1984). Characterization of the intermittent breathing pattern in *Xenopus laevis*. *Journal of Experimental Biology* **110**, 291–309.

Brett SS, Shelton G. (1979). Ventilatory mechanisms of the amphibian, *Xenopus laevis*; the role of the buccal force pump. *Journal of Experimental Biology* **80**, 251–69.

Brown JH, Gillooly JF, Allen AP *et al*. (2004). Toward a metabolic theory of ecology. *Ecology* **85**, 1771–89.

Burggren W (2018). Developmental phenotypic plasticity helps bridge stochastic weather events associated with climate change. *Journal of Experimental Biology* **221**, jeb161984.

Denny MW, Dowd WW (2012). Biophysics, environmental stochasticity, and the evolution of thermal safety margins in intertidal limpets. *Journal of Experimental Biology* **215**, 934–47.

Dell AI, Pawar S, Savage VM (2011). Systematic variation in the temperature dependence of physiological ecological traits. *PNAS* **108**, 10591–6.

Donelson JM, Salinas S, Munday PL, Shama LN (2018). Transgenerational plasticity and climate change experiments: Where do we go from here?. *Global Change Biology* **24**, 13–34.

Emilio MG, Shelton G (1974). Gas exchange and its effect on blood gas exchange in the amphibian, *Xenopus laevis*. *Journal of Experimental Biology* **60**, 567–79.

Emilio MG, Shelton G (1980). Carbon dioxide exchange and its effects on pH and bicarbonate equilibria in the blood of the amphibian, *Xenopus laevis*. *Journal of Experimental Biology* **85**, 253–62.

Feder ME (1983). Responses to acute hypoxia in larvae of the frog *Rana berlandieri*. *Journal of Experimental Biology* **104**, 79–95.

Feder ME, Wassersug RJ (1984). Aerial versus aquatic oxygen consumption in larvae of the clawed frog, *Xenopus laevis*. *Journal of Experimental Biology* **108**, 231–45.

Fonseca EM, da Silva GS, Fernandes M *et al*. (2012). The breathing pattern and the ventilatory response to aquatic and aerial hypoxia and hypercarbia in the frog *Pipa carvalhoi*. *Comparative Biochemistry and Physiology Part A: Molecular, Integrative Physiology* **162**, 281–7.

Gillooly JF, Allen AP, Savage VM *et al*. (2006). Response to Clarke and Fraser: Effects of temperature on metabolic rate. *Functional Ecology* **20**, 400–4.

Gillooly JF, Brown JH, West GB *et al*. (2001). Effects of size and temperature on metabolic rate. *Science* **293**, 2248–51.

Gillooly JF, Gomez JP, Mavrodiev EV *et al*. (2016). Body mass scaling of passive oxygen diffusion in endotherms and ectotherms. *PNAS* **113**, 5340–5.

Glass ML, Boutilier RG, Heisler N (1983). Ventilatory control of arterial P_{O2} in the turtle *Chrysemys picta bellii*: Effects of temperature and hypoxia. *Journal of Comparative Physiology* **151**, 145–53.

Glazier DS (2005). Beyond the '3/4-power law': Variation in the intra- and interspecific scaling of metabolic rate in animals. *Biological Reviews* **80**, 611–62.

Glazier DS (2010). A unifying explanation for diverse metabolic scaling in animals and plants. *Biological Review* **85**, 111–38.

Glazier DS (2014a). Metabolic scaling in complex living systems. *Systems* **2**, 451–40.

Glazier DS (2014b). Scaling of metabolic Scaling within physical limits. *Systems* **2**, 425–50.

Gottlieb G, Jackson DC (1976). Importance of pulmonary ventilation in respiratory control of the bullfrog. *American Journal of Physiology – Legacy Content* **230**, 608–13.

Green SL (2010). *The Laboratory* Xenopus *sp*. CRC Press, Boca Raton, FL.

Greven H, Zanger K, Schwinger G (1995). Mechanical properties of the skin of *Xenopus laevis* (Anura, Amphibia). *Journal of Morphology* **224**, 15–22.

Halsey LG, Butler PJ, Blackburn TM (2006). A phylogenetic analysis of the allometry of diving. *The American Naturalist* **167**, 276–87.

Hastings D, Burggren W (1995). Developmental changes in oxygen consumption regulation in larvae of the south African clawed frog *Xenopus laevis*. *Journal of Experimental Biology* **198**, 2465–75.

Hedrick MS, Hillman SS, Drewes RC, Withers PC (2011). Pulmonary compliance and lung volume varies with ecomorphology in anuran amphibians: implications for ventilatory-assisted lymph flux. *Journal of Experimental Biology* **214**, 3279–85.

Hillman SS, Withers PC (1979). An analysis of respiratory surface area as a limit to activity metabolism in anurans. *Canadian Journal of Zoology* **57**, 2100–5.

Hillman SS, Withers PC (1981). Aerobic contributions to sustained activity metabolism in *Xenopus laevis*. *Comparative Biochemistry and Physiology Part A: Physiology* **69**, 605–6.

Hutchison VH, Miller K (1979). Aerobic and anaerobic contributions to sustained activity in *Xenopus laevis*. *Respiratory physiology* **38**, 93–103.

Hutchison VH, Whitford WG, Kohl M (1968). Relation of body size and surface area to gas exchange in anurans. *Physiological Zoology* **41**, 65–85.

Keeling RF, Garcia HE (2002). The change in oceanic O_2 inventory associated with recent global warming. *PNAS* **99**, 7848–53.

Killen SS, Atkinson D, Glazier DS (2010). The intraspecific scaling of metabolic rate with body mass in fishes depends on lifestyle and temperature. *Ecology Letters* **13**, 184–93.

Leroi AM, Bennett AF, Lenski RE (1994). Temperature acclimation and competitive fitness: an experimental test of the beneficial acclimation assumption. *PNAS* **91**, 1917–21.

Morash AJ, Neufeld C, MacCormick TJ, Currie S (2018). The importance of incorporating natural thermal variation when evaluating physiological performance in wild species. *Journal of Experimental Biology* **221**, jeb164673.

Nagano Y, Ode KL (2014). Temperature-independent energy expenditure in early development of the African clawed frog, *Xenopus laevis*. *Physical biology* **11**, 046008.

Ohlberger J, Mehner T, Holker F (2012). Intraspecific temperature dependence on the scaling of metabolic rate with body mass in fishes and its ecological implications. *Oikos* **121**, 245–51.

Padilla P, Ducret V, Bonneaud C *et al*. (2019). Acclimation temperature effects on locomotor traits in adult aquatic anurans (*X. tropicalis* and *X. laevis*) from different latitudes: possible implications for climate change. *Conservation Physiology* **7**, coz019.

Patterson MR (1992). A mass transfer explanation of metabolic scaling relations in some aquatic invertebrates and algae. *Science* **255**, 1421–3.

R Core Team (2018). *R: A Language and Environment for Statistical Computing*. R Foundation for Statistical Computing, Vienna, Austria. Available from URL: https://www.R-project.org/

Raffel TR, Romansic JM, Halstead NT *et al*. (2013). Disease and thermal acclimation in a more variable and unpredictable climate. *Nature Climate Change* **3**, 146.

Rohr JR, Raffel TR, Blaustein AR *et al*. (2013). Using physiology to understand climate-driven changes in disease and their implications for conservation. *Conservation and Physiology* **1**, cot022.

Rubner M (1883). Ueber den einfluss der korpergrosse auf stoffund kaftwechsel. *Zeitschrift fur Biologie* **19**, 535–62.

Savage VM, Allen AP, Brown JH *et al*. (2007). Scaling of number, size, and metabolic rate of cells with body size in mammals. *PNAS* **104**, 4718–23.

Savage VM, Deeds EJ, Fontana W (2008). Sizing up allometric scaling theory. *PLoS Computational Biology* **4**, e1000171.

Schreer JF, Kovacs KM (1997). Allometry of diving capacity in air-breathing vertebrates. *Canadian Journal of Zoology* **75**, 339–58.

Seebacher F, Tallis JA, James RS (2014). The cost of muscle power production: muscle oxygen consumption per unit work increases at low temperatures in *Xenopus laevis*. *Journal of Experimental Biology* **217**, 1940–5.

Seymour RS (1973). Physiological correlates of forced activity and burrowing in the spadefoot toad, *Scaphiopus hammondii*. *Copeia* **1973**, 103–15.

Shannon P, Kramer DL (1988). Water depth alters respiratory behavior of *Xenopus laevis*. *Journal of Experimental Biology* **137**, 597–602.

Skerratt LF, Berger L, Speare R *et al*. (2007). Spread of chytridiomycosis has caused the rapid global decline and extinction of frogs. *EcoHealth* **4**, 125–34.

Stuart SN, Chanson JS, Cox NA *et al*. (2004). Status and trends of amphibian declines and extinctions worldwide. *Science* **306**, 1783–6.

Tattersall GJ, Currie S, LeBlanc DM (2013). Pulmonary and cutaneous O_2 gas exchange: A student laboratory exercise in the frog. *Advances in Physiology Education* **37**, 97–105.

Tsugawa K (1982). Effects of cold acclimation on the standard metabolic rate and osmotic fragility of erythrocytes in an aquatic anura, *Xenopus laevis*. *Comparative Biochemistry and Physiology Part A: Physiology* **73**, 431–6.

VanBuren CS, Norman DB, Frobisch NB (2018). Examining the relationship between sexual dimorphism in skin anatomy and body size in the white-lipped tree frog. *Litoria infrafrenata* (Anura: Hylidae). *Zoological Journal of the Linnean Society* **186**, 491–500.

West GB, Brown JH, Enquist BJ (1999). The fourth dimension of life: Fractal geometry and allometric scaling of organisms. *Science* **284**, 1677–9.

White CR, Seymour RS (2003). Mammalian basal metabolic rate is proportional to body mass$^{2/3}$. *PNAS* **100**, 4046–9.

Whitford WG (1973). The effects of temperature on respiration in the Amphibia. *American Zoologist* **13**, 505–12.

Withers PC, Hedrick MS, Drewes RC, Hillman SS (2014). Pulmonary compliance and lung volume are related to terrestriality in anuran amphibians. *Physiological and Biochemical Zoology* **87**, 374–83.

Wilson RS, Franklin CE (2002). Testing the beneficial acclimation hypothesis. *TRENDS in Ecology, Evolution* **17**, 66–70.

Wilson RS, James RS, Johnston IA (2000). Thermal acclimation of locomotor performance in tadpoles and adults of the aquatic frog *Xenopus laevis*. *Journal of Comparative Physiology B* **170**, 117–24.

SUPPLEMENTARY MATERIALS

Additional supporting information may be found online in the Supporting Information section at the end of the article.

Table S1 Thermal performance models testing the effects of acclimation temperature (AccTemp) and inverse performance temperature (PerfTemp^{-1}) for the primary controlled-temperature experiment at individual time points.

Table S2 Comparison of estimates for key MTE parameters with and without additional measurements from smaller post-experiment frogs.

Table S3 Breath bout mass- and volume-scaling coefficients ("b") for the primary controlled-temperature experiment.

Table S4 Grouped performance temperatures ("Cool" temperatures [8, 11, 14, & 17°C]; "Warm" temperatures [20, 23, 26, & 29°C]) for comparison of mass- and volume-scaling exponents in the breath bout dataset from the primary controlled-temperature experiment.

Table S5 Average breaths per minute (bpm) in the primary controlled-temperature experiment for frogs in different mass groups and performance temperatures, for comparison with previously published data by Boutilier (1984).

Figure S1 Respirometry device schematic and photos. (a) Schematic of Adafruit Pro Trinket microcontroller and electronic components.

Figure S2 Process of baseline-correcting time series data for oxygen percentage (a,b) and air flow rate (c,d) for a single representative breath bout.

Figure S3 Thermal performance curves across all time points in the primary controlled-temperature experiment.

Figure S4 Thermal performance curves for all metabolic proxies for one, four, and eight days post-acclimation in the primary controlled-temperature experiment.

Figure S5 Characteristic breathing patterns of *X. laevis* observed in this study.

Figure S6 Proportion cutaneous respiration as a function of log-transformed frog mass, showing all measurements including the eight smaller frogs measured after the primary controlled-temperature experiment was completed.

Figure S7 Dissolved oxygen availability and proportion of respiration performed cutaneously as functions of temperature in the primary controlled-temperature experiment.

Cite this article as:

McWhinnie RB, Sckrabulis JP, Raffel TR (2021). Temperature and mass scaling affect cutaneous and pulmonary respiratory performance in a diving frog. *Integrative Zoology* **16,** 712–28.